




# Perovskites used as cathode in solid oxide fuel cells synthesized by solution combustion synthesis (SCS)

Thais dos Santos Haas<sup>1,\*</sup> , Willians Lopes de Almeida<sup>2</sup>, Felipe Antonio Lucca Sánchez<sup>1</sup>, and Vânia Caldas de Sousa<sup>1</sup>

<sup>1</sup>Advanced Ceramics Laboratory-Graduate Program in Mining, Metallurgical and Materials Engineering, Federal University of Rio Grande do Sul, Porto Alegre, RS 91501-970, Brazil

<sup>2</sup>Federal Institute of Education, Science and Technology of Amapá, Macapá, AP 68909-398, Brazil

Received: 29 March 2023

Accepted: 27 June 2023

Published online:

15 July 2023

© The Author(s), under exclusive licence to Springer Science+Business Media, LLC, part of Springer Nature 2023

## ABSTRACT

Lanthanum ferrites present electrical and magnetic properties that enable their use in several areas. Specifically, lanthanum ferrites doped with cobalt and strontium have electrical conductivity and thermal stability, which enable their use as electrodes (cathode) in solid oxide fuel cells and as catalysts in oxygen separation membranes. This study aimed to investigate the effect of the fuel concentration and calcination temperature over the synthesis of  $\text{La}_{0.6}\text{Sr}_{0.4}\text{Co}_{0.8}\text{Fe}_{0.2}\text{O}_3$  nanopowders through solution combustion synthesis (SCS) using sucrose ( $\text{C}_{12}\text{H}_{22}\text{O}_{11}$ ) as fuel. Therefore, the powder was obtained using oxidant and reductant reagents in a stoichiometric amount (1:1) and with an excess of reducing reagent in the composition (1:2) and thermal treatment in several temperature ranges, 1100 and 1200 °C, was performed. As a result, the samples calcined at 1200 °C showed the best structural characteristics concerning the other temperatures used, with an average crystallite size of 37 nm for the 1:1 sample and 42 nm for the 1:2 sample. The conductivity of the materials tends to increase with increasing temperature and excess of fuel. At 500 °C, in the 1:1 sample,  $2.61 \times 10^{-4}$  S/cm was obtained and in the 1:2 sample,  $11.4 \times 10^{-4}$  S/cm. Given the findings obtained in this work report, the fuel excess increases crystallite size and conductivity and reduces band gap and activation energy, emphasizing a considerable influence of the content of fuel used in SCS in the evaluated properties.

## 1 Introduction

In recent years, several studies have been developed to investigate materials with perovskite structure due to their mixed conduction mechanisms when doping

elements are inserted into the structure [1]. Among a wide range of materials studied, lanthanum ferrites doped with cobalt and strontium (LSCF) have been highlighted and shown to be very promising in the field of advanced ceramics, presenting good

Address correspondence to E-mail: haasthais@gmail.com

characteristics such as high catalytic activity in the oxygen reduction reaction and chemical stability at intermediate temperatures, in addition to good electrical, magnetic, and thermal properties [2, 3]. Their wide applications range from use as cathode material in Solid Oxide Fuel Cells (SOFCs) to oxygen separation membranes and membrane reactors for syngas production and partial oxidation of hydrocarbons [4, 5]. As concerns SOFC application, many studies [6, 8–11] have been developed and have shown that the increase in the cobalt content tends to increase the conductivity of the ferrite.

According to Jiang [8], lanthanum ferrites doped with cobalt and strontium (LSCF) are the most popular and representative mixed ionic and electronic conduction electrode (MIEC) material for SOFC application operating at intermediate temperature (600–800 °C).

The electronic structure of LSCF is a combination of lanthanum ferrite doped with strontium (LSF) and lanthanum cobaltite doped with strontium (LSC). LSC and LSF have similar crystal structure but differ in their electronic structure [8].

The composition containing the highest cobalt concentration stands out for having higher electrical conductivity. This is because cobalt ions at the B site, in the  $ABO_3$  perovskite structure, appear to have lower binding energy with oxygen than Fe ions [9]. On the Other hand, Fe ions control the migration of oxygen ions in the structure, in addition to controlling the thermal expansion coefficient (TEC) of the material.

Some scientific works [6–8] describe that the composition,  $La_{0.6}Sr_{0.4}Co_{0.8}Fe_{0.2}O_3$ , which is the object of this study, presents an interesting compromise of properties, in terms of good electronic conduction and a discreet thermal expansion, (TEC) when the focus is on its application as a cathode in SOFCs, for example.

In the perovskite structure ( $ABO_3$ ), the elements of the A site are rare earths and alkaline earth metals with coordination number 12. In contrast, the transition metals occupy the B site with coordination number 6. The A and B elements are cations in which the A element has the largest ionic radius of the structure, while O (oxygen) is the anion [10]. At room temperature and without the addition of dopants, perovskite usually presents a cubic structure. With the addition of dopant elements, a distortion in the structure occurs. The partial substitution of A-site

cations for lower valence state cations increases the oxygen vacancies in the system. This increase in oxygen vacancies preserves the neutrality of the system, which results in improved ionic conductivity with better catalytic properties. As for the B site, the substitution of ions with similar size but lower valence can be used to adjust the concentration of oxygen vacancies. The materials have good electronic conductivity due to the mixed valence states of the different constituent elements present in the B site of the perovskites.

Several methods have been proposed to synthesize materials with this structure, such as electrospinning [11], sol-gel, Pechini [12], and solution combustion synthesis [13–15], besides other methods that aim to obtain better structural and morphological characteristics and, consequently, better properties. According to Sousa [13], in relation to other methods of powder synthesis, the combustion reaction is considered fast, simple, economical and makes it possible to obtain fine, homogeneous, and, in certain cases, crystalline powders, without the risk of contamination, because it does not require grinding steps.

Besides the choice of synthesis method, other factors influence the morphological and structural properties of the powders. In solution combustion synthesis, among the wide range of fuels available for application are glycine [4, 15–17], urea [15, 17], citric acid [15], and sucrose [15, 18]. The type and amount of fuel selected have a direct influence on the synthesis process, such as the reaction rate, gas generation, and reaction temperature. These parameters determine the characteristics of the material obtained such as crystallinity, particle size, and formation of adjacent phases, thus altering the final properties of the powders obtained, such as conductivity.

Although solution combustion synthesis has already been used to synthesize the lanthanum ferrites doped with cobalt and strontium (LSCF), no works were found in the literature in which sucrose has been used to obtain ferrite by solution combustion synthesis in the composition and with the same percentage of dopants used in the present work. Furthermore, the effect of sucrose variation on the properties of LSCF powders hasn't been done yet.

Therefore, the present work proposes the synthesis of  $La_{0.6}Sr_{0.4}Co_{0.8}Fe_{0.2}O_3$  nanopowders by solution combustion synthesis using sucrose as fuel, observing the effect of the fuel concentration and calcination

temperature over the phase formation, electrical conductivity, optical band gap, crystallite size, and activation energy of the powders obtained.

## 2 Experimental

Solution combustion synthesis (SCS) was the method used to obtain the powders. The fuel chosen for the process was sucrose ( $C_{12}H_{22}O_{11}$ ), as an easily obtainable and low-cost material, besides the ability to obtain powders with smaller particle size, according to previous researches [19]. For the realization of the reaction, oxidant and fuel were used in stoichiometric quantity (1:1) and fuel with 100% excess in the solution (1:2).

To produce the  $La_{0.6}Sr_{0.4}Co_{0.8}Fe_{0.2}O_3$  (represented by the acronym LSCF) powders, several chemical reactions were performed using La ( $NO_3$ )<sub>3</sub>·6H<sub>2</sub>O (lanthanum (III) nitrate hexahydrate ( $\geq 99.0\%$ )), Sr ( $NO_3$ )<sub>2</sub> (strontium (II) nitrate ( $\geq 98\%$ )), Co ( $NO_3$ )<sub>2</sub>·6H<sub>2</sub>O (cobalt (II) nitrate hexahydrate (98%)), Fe ( $NO_3$ )<sub>3</sub>·9H<sub>2</sub>O (iron (III) nitrate nonahydrate ( $\geq 98\%$ )), and  $C_{12}H_{22}O_{11}$  (sucrose ( $\geq 99.5\%$ )).

Using the method described by Jain [20] and Sousa [13], proportions of the cation precursor reagents (nitrates) and reductant reagents (sucrose-fuel) were used based on the total valences of the elements, where, in modulus, the sum of the valences of the oxidizing elements (nitrates) divided by the sum of the valences of the reducing element should be equal 1.

The materials were weighed separately and then mixed with enough distilled water, necessary to dissolve the reagents, in a round-bottomed glass balloon. To perform the synthesis, the balloon was placed on a heating mantle inside an exhaust hood.

The solutions were kept at 110 °C for 1 h with an inertia of  $\pm 40$  °C for water evaporation until they turned into a gel, then raising the temperature to 280 °C. Flame propagation started at 280 °C and continued for approximately 15 min with the 1:1 composition, and 5 min with the 1:2 composition, until powder formation.

After synthesis, the powders were deagglomerated on a #200 mesh sieve. Then, they were calcined at different temperatures: 900 °C, 1100, and 1200 °C, maintaining the plateau of 1 h and the heating rate of 10 °C/minute. The calcination below 1100 °C was performed in a Sanchis furnace (maximum

temperature limit of the furnace) and above 1100 °C in a Carbolite HTF 17/5 furnace.

Thermal analysis, thermogravimetric analysis (TGA), and differential thermal analysis (DTA) of the powder obtained were performed in a Parkin Elmer TGA 4000 thermal analyzer. The samples were heated in the temperature range of 30 to 990 °C, with a heating rate of 10 °C/min in N<sub>2</sub> atmosphere.

The crystallinity of the powders obtained (before and after thermal treatment) was analyzed by X-ray diffraction (XRD). The measurements were performed by a Siemens X-ray diffractometer (BRUKER AXS) D-5000 with a curved graphite monochromator in the secondary beam operating at a voltage of 40 kV and current of 30 mA, with Cu K $\alpha$  radiation ( $\lambda = 1.5406$  Å) and scanning in the angular range of 10 to 70° of 2 $\theta$ . The samples were analyzed at a step interval of 0.05° for 1 s, with divergence and anti-scattering slits of 1° (degree) and a reception slit of 0.6 mm. For phase identification, the program X'Pert HighScore Plus 2012 version 3.0 was used.

In addition, the crystallite sizes of the powders were identified using Debye–Scherrer's Eq. (1) [21]. In the equation,  $\beta$  = width at half-height of the diffraction peak determined in radians (described by the acronym FWHM),  $D$  = crystallite size,  $\lambda$  = X-ray wavelength (1.5406 Å),  $\theta$  = Bragg's angle, and  $K$  (we assume the value of 0.9) is the correction factor, which can vary depending on the shape of the crystallites presumed to be in the sample.

$$D = \frac{K\lambda}{\beta \cos\theta} \quad (1)$$

The samples were also analyzed by transmission electronic microscopy (TEM), in a Thermofisher microscope, Tecnai T20 model, with an applied voltage of 200 kV and TIA software for evaluation of the captured images.

Using an oven coupled to an INTI controller, model FTK 1100, measurements of electric current and electric voltage in direct current as a function of temperature were performed on the 1:1 and 1:2 LSCF powders calcined at 1200 °C. For the test, the temperature was varied between 30 and 500 °C and, by different voltage ranges, the current was determined. The powder was deposited, without compaction, on a sample holder (alumina ring) with an internal diameter of 5.07 mm and an area of 20.18 mm<sup>2</sup>. Aluminum was selected as an electrode.

From the current and voltage measurements, it was possible to calculate, through Ohm's law, the electrical resistance, the resistivity, and the electrical conductivity of the material.

The area of the material was determined from the measurement of the inner diameter of the alumina ring used as a sample holder for the electric characterization.

After determining the aforementioned data, the Arrhenius curve was drawn, from which it was possible to determine the activation energy ( $E_a$ ) of the material, calculated using the Arrhenius equation, Eq. (2), in which  $C_m$  is the material constant,  $T$  is the absolute temperature, and  $k$  is the Boltzmann constant ( $1.380649 \times 10^{-23} \text{ m}^2 \cdot \text{kg} \cdot \text{s}^{-2}\text{k}^{-1}$ ).

$$\sigma = \frac{C_m}{T} \exp\left(\frac{-E_a}{kT}\right) \quad (2)$$

The indirect band gap of the produced materials was determined by Tauc Plot method [22] measuring the UV-Vis diffuse reflectance spectra (UV-Vis DRS), assisted by a spectrophotometer Shimadzu UV2450PC using an ISR-2200 Integrating Sphere Attachment. The experiments were performed at room temperature in the range of 300 at 800 nm. The baseline in the solid state was obtained using  $\text{BaSO}_4$  (Wako Pure Chemical Industries, Ltd.). For all experiments, the obtained materials were treated as powder.

### 3 Results and discussion

#### 3.1 Thermal analysis by TGA and DTA

Figure 1a, b show the thermal behavior of the  $\text{La}_{0.6}\text{Sr}_{0.4}\text{Co}_{0.8}\text{Fe}_{0.2}\text{O}_3$  (LSCF) powder through the TGA and DTA curve of the 1:1 and 1:2 samples, respectively. The test, performed at a temperature between 30 and 990 °C, showed, through the TGA curve, that there was a weight loss of 10% of sample 1:1 and 22% of sample 1:2. In the analysis through the DTA curve, several exothermic reactions are observed in the 1:1 composition, the peak at 600 °C being prominent. For the 1:2 composition, four exothermic reactions are observed at 150 °C, 500 °C, 700 °C, and 900 °C. The peak is most intense at 500 °C.

The weight loss and the various exothermic events occurring at different temperature ranges are possibly due to the removal of humidity from the

powders, the decomposition of the nitrates and sucrose portion, and partial burning of the oxygen present in the structure due to the creation of vacancies with the addition of strontium at the A position.

By inserting more sucrose in the structure, a greater amount of gases was generated during the synthesis, preventing the complete combustion of some nitrates. Therefore, the TGA curve of the synthesized powders showed a significant weight loss of the 1:2 sample, because the increase in the temperature during the analysis could result in the total decomposition of these nitrates.

When analyzing the DTA curves of Fig. 1a, b, it is observed that there is some similarity regarding the temperatures at which the exothermic reactions occur. The first reaction, which occurs in the 150 °C range for both samples, is possibly due to the elimination of moisture present in the ferrite powders. However, a distinct behavior is observed that occurs only in sample 1:1 (Fig. 1a) at 250 and 350 °C and is possibly responsible for the decomposition of nitrates that were still present in this sample even after the combustion reaction and that were no longer present in sample 1:2. Between 400 and 650 °C, exothermic peaks are observed for sample 1:1 and a single intense peak for sample 1:2. For both, this range represents the formation of the crystalline LSCF phase, in addition to decomposition of  $\text{C}_{12}\text{H}_{22}\text{O}_{11}$  [19], and elimination of gases such as  $\text{CO}_2$  [13]. Considering that both samples have the same composition, but with the 1:2 sample having twice as much fuel inserted in the solution, the distinct behavior in this temperature range implies the formation of a greater amount of gases and a greater amount of fuel to decompose, noting also that, in this temperature range, the loss in weight for the 1:1 sample is 6%, and for the 1:2 sample 13%.

According to Biswas [18] in a study of the preparation of the  $\text{LaNiO}_3$  system by solution combustion synthesis using sucrose as fuel, the high exothermic peak in the 500 °C temperature range would be linked to the slow combustion of the carbon element present in the fuel.

Stevenson et al. [4] in a study on the electrochemical properties of mixed conduction perovskites of the type  $\text{La}_{1-x}\text{M}_x\text{Co}_{1-y}\text{Fe}_y\text{O}_{3-\delta}$  ( $\text{M} = \text{Sr}, \text{Ba}, \text{Ca}$ ) prepared by the solution combustion synthesis, reported, through TGA analysis under air atmosphere, that for the structure  $\text{La}_{1-x}\text{Sr}_x\text{Co}_{1-y}\text{Fe}_y\text{O}_{3-\delta}$  the magnitude of

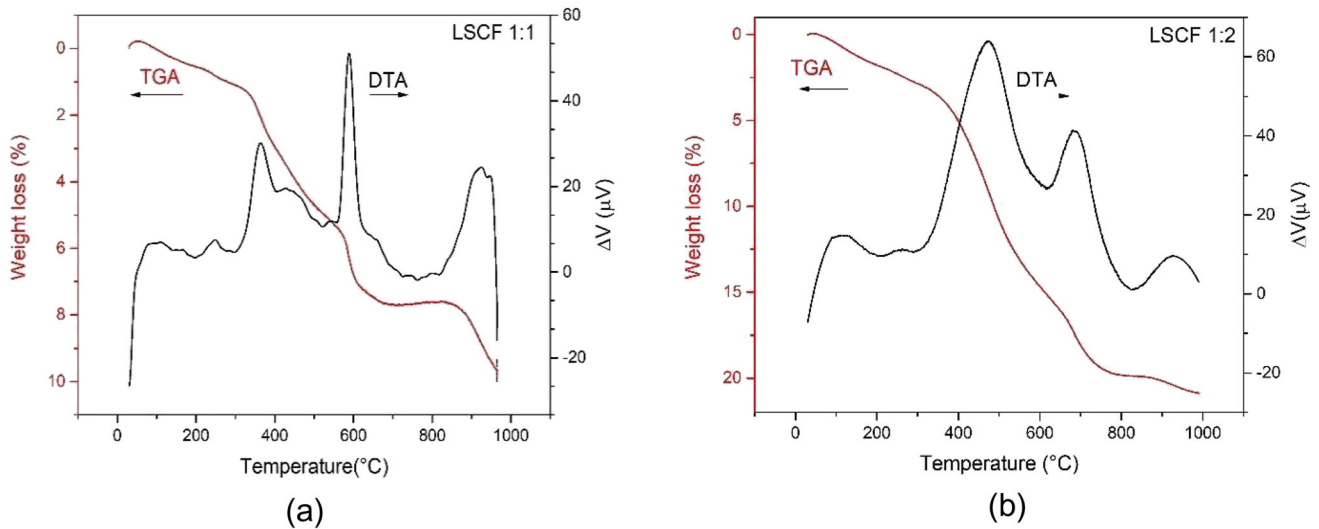


**Fig. 1** TGA and DTA curves of LSCF powder obtained by combustion: **a** sample 1:1, **b** sample 1:2

oxygen loss during heating is highly composition dependent and tends to increase with increasing strontium content in the A site. For a structure with 40% strontium, significant weight loss was observed between 600 and 1200 °C.

A study by Tai et al. [9], using TGA analysis measured under air atmosphere, demonstrated the influence of the strontium content on the weight loss of the structure as a function of temperature and also the oxygen content as a function of temperature. They concluded that for an LSCF system with 40% strontium in the A position, there was a loss of 0.12 mols of oxygen from the structure at 1000 °C and significant weight loss above 600 °C. This result was also linked to the exothermic peaks present at 900 °C for samples 1:1 and 1:2.

Sample 1:2 also presented an exothermic peak in the range of 700 °C representing the decomposition of the element strontium nitrate [23].

In another study [15], aiming to study the effect of propellant on the properties of LSCF, the  $\text{La}_{0.7}\text{Sr}_{0.3}\text{Co}_{0.5}\text{Fe}_{0.5}\text{O}_3$  was obtained by solution combustion synthesis using different fuels in a stoichiometric amount. In their TGA and DTA analysis, the curves represented by powder synthesized with sucrose showed that the weight loss was approximately 22%, as was observed for the 1:2 sample, and the DTA curve showed an intense exothermic peak at 370 °C indicating the decomposition of  $\text{C}_{12}\text{H}_{22}\text{O}_{11}$  that was still present after synthesis (incomplete combustion).

### 3.2 Identified phases by XRD

The X-ray diffractograms of the 1:1 and 1:2 compositions are shown in Fig. 2a, b, respectively. In the LSCF 1:1 composition, it was possible to identify the beginning of the formation of the  $\text{La}_{0.6}\text{Sr}_{0.4}\text{Co}_{0.8}\text{Fe}_{0.2}\text{O}_3$  phase immediately after synthesis in which the  $\text{Co}_3\text{O}_4$  phase is also present. On the other hand, the 1:2 composition, analyzed after synthesis, showed only  $\text{Sr}(\text{NO}_3)_2$  diffraction peaks according to JCPDS sheet 76-1375.

For the 1:2 composition, the temperature required for decomposition of this nitrate was not reached during the SCS that, according to research conducted by Culas [23], the decomposition temperature of strontium nitrate is 918.3 K (645.15 °C). Furthermore, the excess of fuel added in the reaction generated a greater amount of gases that prevented the temperature rise in the reaction from reaching the decomposition temperature of strontium nitrate [19, 24].

Then, it was observed, for the 1:2 composition, that as the heat treatment temperature is increased, the decomposition and reaction of strontium nitrate occurs. On the other hand, after heat treatment at 900 °C, this composition presented, besides the LSCF phase with rhombohedral structure, according to JCPDS data sheet 48-0124, a  $\text{Co}_3\text{O}_4$  phase with cubic structure, according to JCPDS data sheet 74-2120. As the temperature was increased to 1100 °C, the LSCF and  $\text{Co}_3\text{O}_4$  phases continued to be observed, but the peaks intensity of the  $\text{Co}_3\text{O}_4$  phase was smaller.



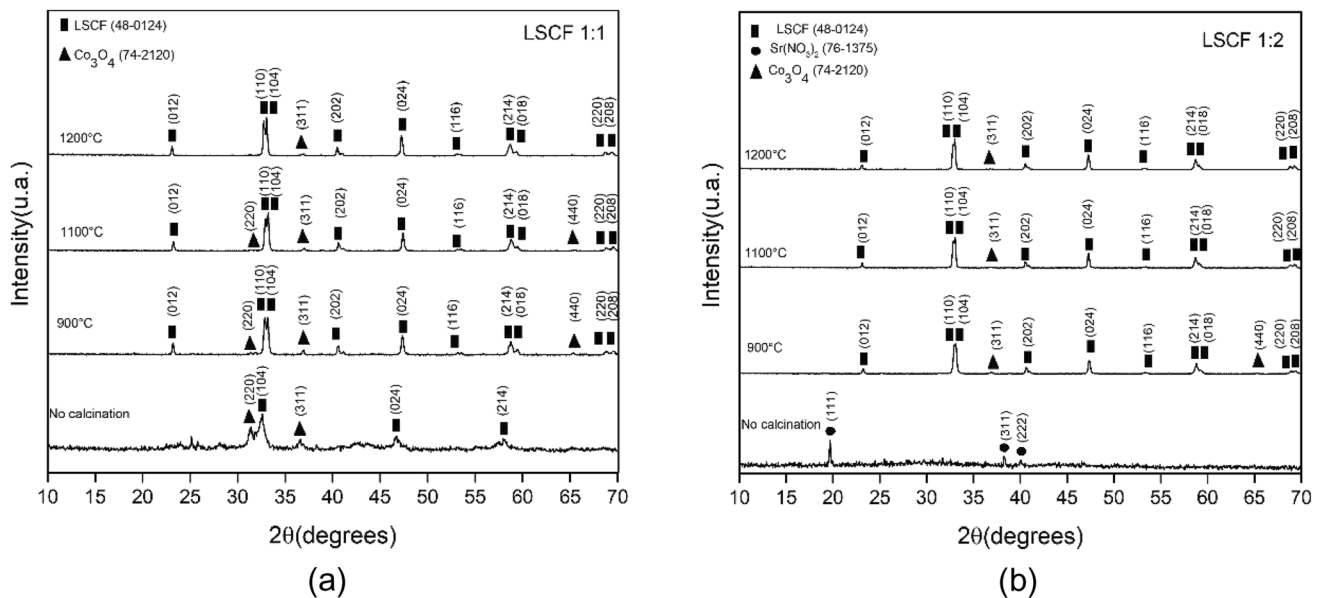


**Fig. 2** X-ray diffractograms of the material obtained by SCS: **a** 1:1 composition, **b** 1:2 composition

A similar situation was analyzed for the 1:1 composition, but the  $\text{Co}_3\text{O}_4$  phase presented more intense peaks. The intensity of the peaks of a  $\text{Co}_3\text{O}_4$  phase was decreased as the heat treatment temperature increased.

After calcining the powders at 1200 °C, it was observed that there was still a  $\text{Co}_3\text{O}_4$  peak in both samples, which can be seen in Fig. 2b. The  $\text{Co}_3\text{O}_4$  peak in 1:2 sample is smaller, indicating that the 1:2 composition presented a more pure LSCF phase than the 1:1 composition.

It was also observed that, for both samples, the higher the treatment temperature, the smaller was the value of the width of the diffraction peak of highest intensity, indicating greater crystallinity. Figure 3a presents the magnification of diffraction peaks of highest intensity 1:1 and 1:2 compositions after heat treatment at 1200 °C. It's observed that the peaks of the 1:2 composition are narrower than the 1:1 composition, indicating that the 1:2 powder is more crystalline than the 1:1 powder.

It is also observed that the increase in fuel content tends to reduce the intensity of the peak related to the presence of cobalt oxide, as shown in Fig. 3b.

From the Debye–Scherrer Eq. (1) [21], the average crystallite size of the powders was carried out from all diffraction peaks of the LSCF phase, as specified in Table 1. According to the results, the increase of the heat treatment temperature in the 1:1 and 1:2 composition does not significantly change the crystallite

size. On the other hand, increasing the fuel concentration tends to increase the size of the crystallites. The fuel content had more influence on the size of the crystallites than the calcination temperature. This behavior was also observed by other authors using the same synthesis method to obtain other components, such as mayenite [25]. The excess of oxidizers (fuels) contributes to the formation of more heat and the release of more gases that are not properly dissipated, resulting in an increase in the size of the crystallite, as demonstrated by Tarrago et al. [19]

In addition to the variation between fuel-to-oxidizer ratio and calcination temperature, other factors determine the crystallite size. In the literature, several different results are found depending on the parameters used. In the work performed by Chanquía et al. [26], ferrites were also synthesized by SCS using glycine as fuel in addition to ammonium nitrate. The ferrites were synthesized and calcined at various temperatures for a period of 6 h and presented crystallites size of 32.7 nm at 700 °C and 45.3 nm at 800 °C. Similar values to those described in this work. In other works, the crystallite size determined by Williamson–Hall and Scherrer methods, of the LSCF synthesized by SCS using sucrose and other fuels, was smaller than 20 nm. Conceição et al. [15] synthesized  $\text{La}_{0.7}\text{Sr}_{0.3}\text{Co}_{0.5}\text{Fe}_{0.5}\text{O}_3$  by SCS using various fuels, including sucrose in proportion 1:2. In this work, the powders synthesized using sucrose as fuel presented 19.7 nm of crystallite size after calcination

**Fig. 3** Magnification of the most intense peaks (a) and the  $\text{Co}_3\text{O}_4$  peaks (b) obtained by X-ray diffraction patterns of the 1:2 (1200 °C) and 1:1 (1200 °C) compositions

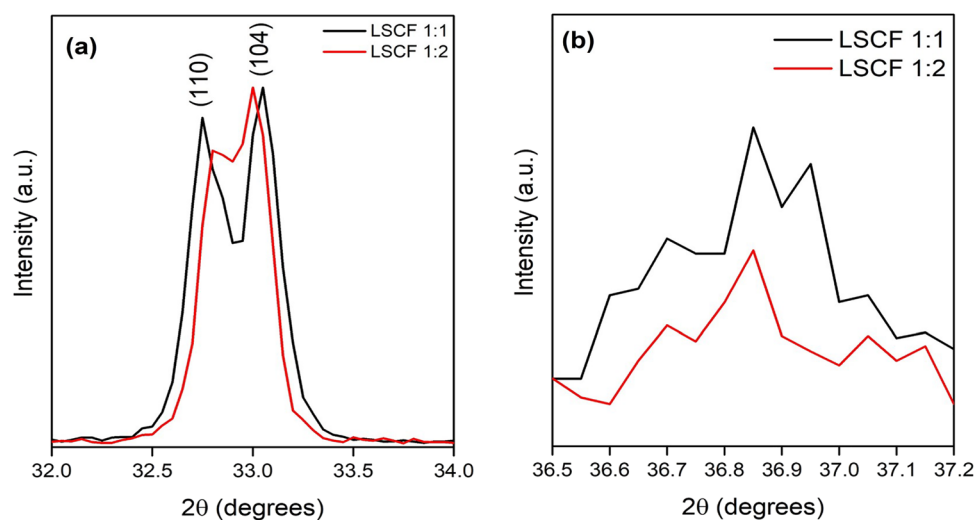


**Table 1** Crystallite size of powders after heat treatment for 1 h

Composition (oxidant:reductant)	Heat treatment temperature (°C)	Average crystallite size (nm)
1:1	900	40
1:1	1100	38
1:1	1200	37
1:2	900	45
1:2	1100	41
1:2	1200	42

at 750 °C/10 hours. The same crystallite size was obtained by Jamale et al. [14] with the  $\text{La}_{0.6}\text{Sr}_{0.4}\text{Co}_{0.8}\text{Fe}_{0.2}\text{O}_3$  powders synthesized by SCS using glycine as fuel and calcination at 650 °C/5 hours with the same proportion of oxidant/reductant (1:2).

As the samples sintered at 1200 °C showed greater purity, emphasis was placed on the more detailed characterization of the 1:1 and 1:2 fuel-to-oxidizer ratio calcined at this temperature.

### 3.3 Particle analysis by TEM

From the images obtained by TEM of LSCF powders calcined at 1200 °C (Fig. 4), it can be seen that the solution combustion synthesis favors the nanoparticles obtained, measuring below 20 nm. In addition, by increasing the amount of fuel (LSCF 1:2), the average particle size tended to increase (Fig. 5) with well-defined morphology predominating the formation of small spheres. In these samples, the occurrence of coalescence that may represent the beginning of sintering is also observed. On the other hand, the 1:1 sample showed agglomerates of particles which made it difficult to identify the particle's

morphology. This behavior can be attributed to the fact that there is a greater trapping of gases in the precursor solution of the 1:2 sample, caused by excess fuel in the precursor solution, which made it more viscous. In addition, excess fuel tends to form a more porous structure, which may also have implications in the optoelectronic properties. According Tarragó et al. [19], in a study of influence of fuel on morphology of LSM powders obtained by SCS, the use of sucrose makes the solution more viscous, promoting the retention of gases that delineated the morphology of the aggregates.

### 3.4 UV-Vis DRS measurements

The diffuse reflectance spectra of samples LSCF 1:1 and LSCF 1:2 shown in Fig. 5, reveal that both samples have similar photophysical behavior, from the perspective of the response to diffuse reflectance, being significantly transparent at wavelengths above 600 nm. From 550 nm, both samples present an intense light absorption and stabilize their light absorption at wavelengths below 400 nm.

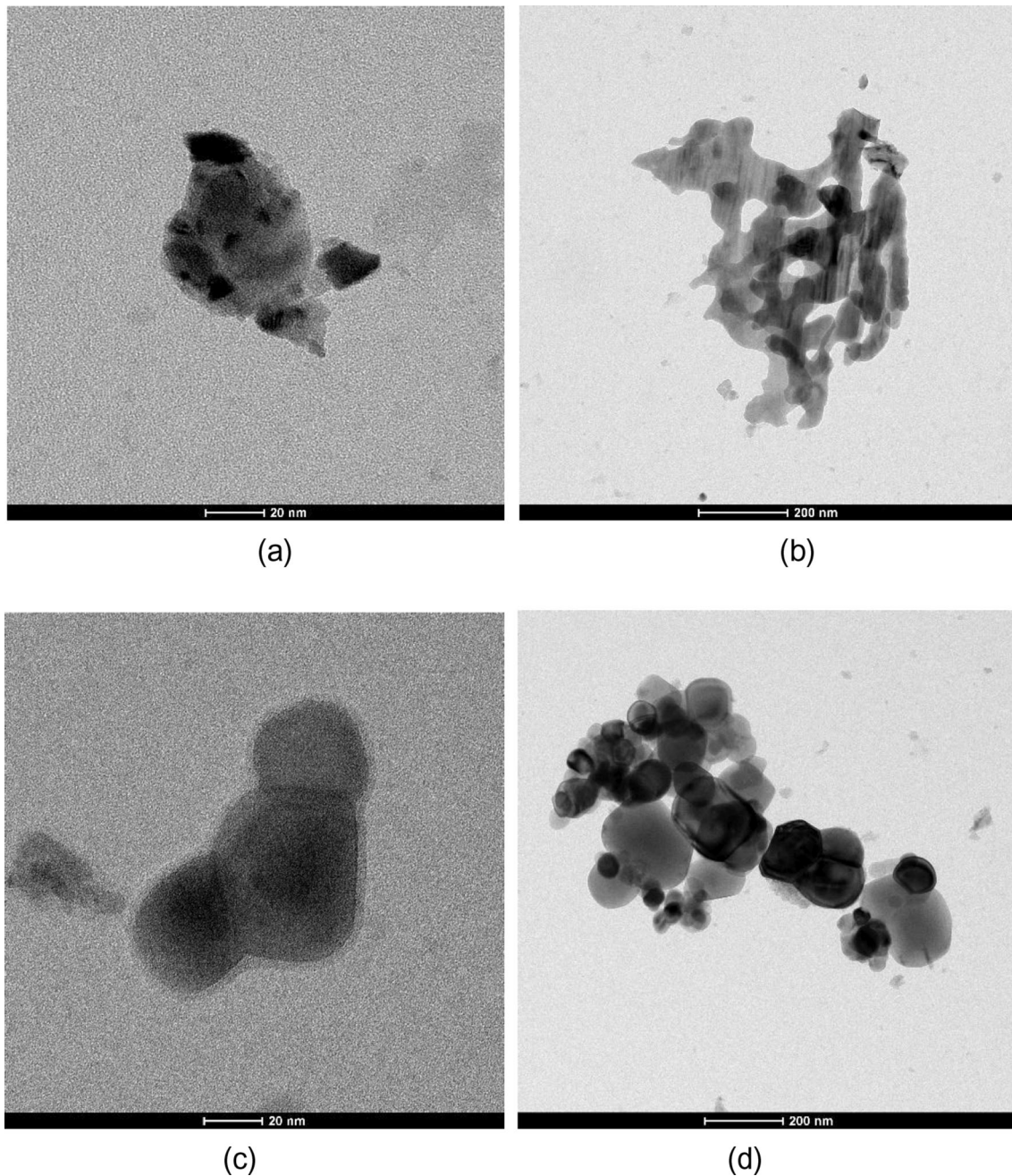


**Fig. 4** TEM of LSCF powders calcined at 1200 °C: **a** and **b** LSCF 1:1; **c** and **d** LSCF 1:2

On the other hand, according to Fig. 6a, b, the indirect band gaps, determined by the Tauc Plots method, allowed finding a certain difference between the band gaps found. LSCF 1:1 showed a band gap of 1.51 eV while the band gap of sample LSCF 1:2 was 1.47 eV. Can be observed a reduction in the band gap with the increase in the fuel content. This result could be explained by the increase in the crystallite size, as it was demonstrated by other researchers [25, 27, 28]

that the decrease in the crystallite size tends to increase the band gap, due to the enhancement of quantum confinement effect in the nanometric scale.

### 3.5 Electrical conductivity measurements, activation energy, and band gap

Through measurements of the electric current and voltage in direct current mode as a function of



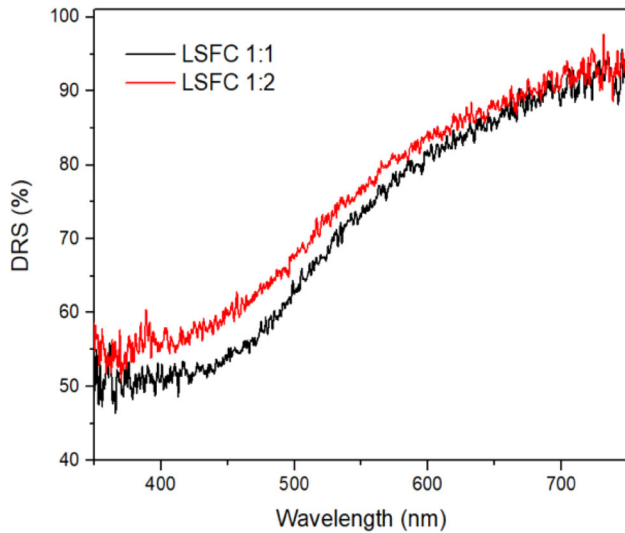


**Fig. 5** Diffuse reflectance spectra of ferrites powders with different amounts of fuel and calcined at 1200 °C

temperature realized in the powders calcined at 1200 °C, the conductivity versus temperature curves and Arrhenius plot were obtained, presented in Figs. 7 and 8, respectively.

From the results, it can be observed that the LSCF powder with excess fuel presents higher electrical conductivity compared to the LSCF 1:1 sample. As shown in Fig. 7; Table 2, the conductivity of the sample LSCF 1:2 tends to increase above 300 °C, reaching a conductivity of  $11.4 \times 10^{-4}$  S/cm at 500 °C. On the other hand, the sample without excess of fuel, LSCF 1:1, remained with the conductivity constantly close to 0 S/cm until 300 °C, after which temperature the conductivity value started to

**Fig. 6** Tauc's plot for indirect band gap energies of LSCF Synthesized with different amounts of fuel **a** and **b** calcined at 1200 °C

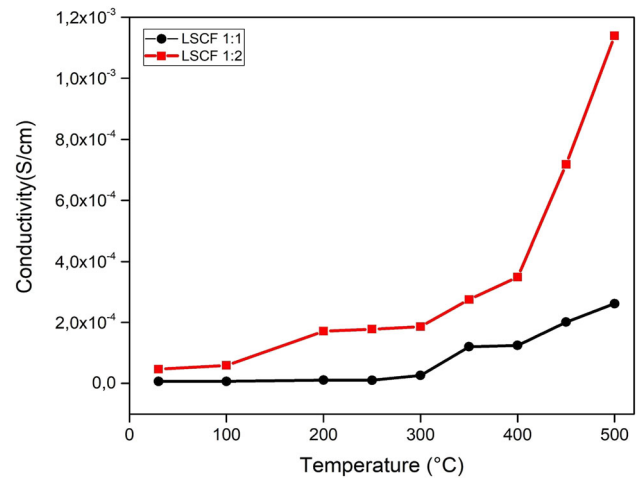
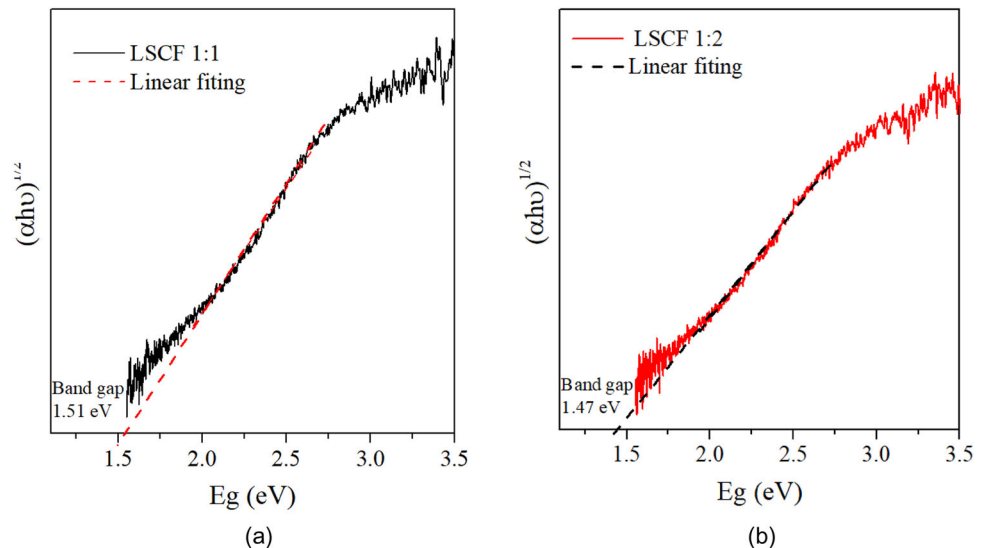


**Fig. 7** Conductivity versus temperature curve of the LSCF powders calcined at 1200 °C

increase, reaching  $2.61 \times 10^{-4}$  S/cm at 500 °C, with a value almost five times lower than the value observed for the other sample.

It is important to consider that the material analyzed was a powder that was lightly compacted in a sample holder, that means, with low densification, which implies the presence of pores and air that lead to an increase in the resistivity values. Therefore, the values presented here must be compared with materials analyzed under the same sample preparation conditions. The Arrhenius conductivity curves were based on the electrical measurements shown in Table 2 with the application of 6 V for LSCF 1:1 and 4 V for LSCF 1:2.

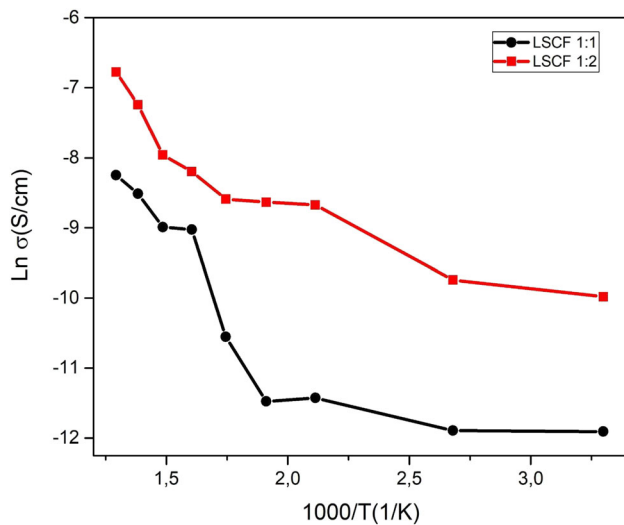


**Fig. 8** Arrhenius conductivity plot of the LSCF powders, showing the logarithm of conductivity as a function of the inverse of temperature

Conceição [15] obtained  $\text{La}_{0.7}\text{Sr}_{0.3}\text{Co}_{0.5}\text{Fe}_{0.5}\text{O}_3$  powders by combustion using various fuels. When using sucrose as fuel, the activation energy values ranged between 0.163 and 1.026 eV due to the variation in the material synthesis temperature, which varied between 950 and 1100 °C, respectively. Using urea as fuel, the activation energy values varied between 0.177 eV and 1.342 eV for the same range of synthesis temperature variation.

In relation to other values for activation energy found in the literature, it is difficult to perform a direct comparison of the results for this material, since the proportion of doping used is directly influenced by the properties of the charge carriers of the perovskite. The synthesis method chosen, as well as the type of fuel used, also influence the results, since the time and temperature to obtain the powder as well as the temperature and time of synthesis influences the crystallinity of the material.

It can also be found that a higher activation energy is rightly observed for the less conductive material, which is in accordance with the conductivity

determined by the Arrhenius Eq. (2). The activation energy values indicate that the reaction mechanism of oxygen reduction is related to charge transfer and diffusion processes [29]. Therefore, the lower the value of activation energy, the greater the probability of electrical conduction.

There are many reasons that can explain the occurrence of increased conductivity. One of the most relevant is that small polarons prevail with an increase in conductivity as their mobility is thermally activated. This is attributed to a substantial increase of thermally-induced oxygen loss, decreasing not only the concentration but also the mobility of electronic carriers at high temperatures [15]. In addition, Co ions on the B site appear to have a smaller binding energy for oxygen than Fe ions, due to the greater degree of oxygen deficiency in LSCF perovskites with high Co content. The substitution of Fe for Co alters not only the crystal structure but also the orbital configuration of valence electrons. Furthermore, the increase in the conductivity may also result from the type of charge carriers and their density [9].

In addition, Fig. 9 shows the relationship between crystallite size, conductivity, and band gap of powders calcined at 1200 °C. This relation reveals that the excess of fuel increases the crystallite size and conductivity and reduces the band gap, emphasizing that there is a significant influence of the content of fuel used in SCS in the properties previously discussed.

In the work carried out by Hung et al. [30] it was demonstrated that the LSCF perovskite, with a smaller crystallite size, had higher activation energy. These authors attributed this effect to oxygen vacancies, which tend to increase the band gap mobility of charge carriers between the cation of the B site and the oxygen ion. This is corroborated by the results of this study since the LSCF 1:2 sample has a larger crystallite size, lower activation energy, and band gap.

At this point, it is clear that there is a relationship between the structure and properties of the ferrite produced under varying amounts of fuel. According

**Table 2** Conductivity and activation energy of the LSCF powders

Composition (oxidant:reductant)	Conductivity at 30 °C (S/cm)	Conductivity at 500 °C (S/cm)	Activation energy (eV)
1:1	$0.0672 \times 10^{-4}$	$2.61 \times 10^{-4}$	0.15
1:2	$0.4630 \times 10^{-4}$	$11.40 \times 10^{-4}$	0.13

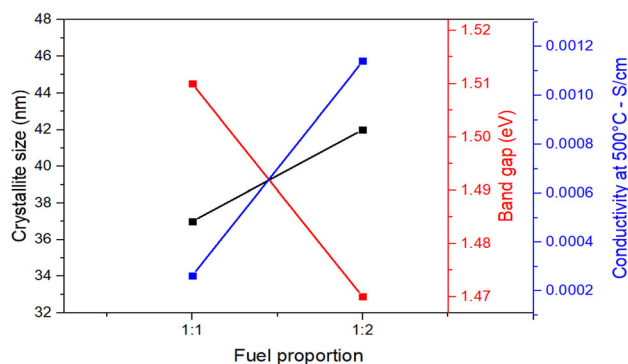


**Fig. 9** Correlation between crystallite size, electrical conductivity at 500 °C, and optical band gap of perovskite powders calcined at 1200 °C with different amounts of fuel used during SCS.

to Fig. 3b, it is clear that the increase of sucrose in the SCS process leads to a reduction in the presence of cobalt oxide which means, that this process variation promotes the migration of cobalt ions from the oxide structure to the perovskite phase and these phenomena produce a material with higher electrical conductivity, increase in the crystallite size and the reduction in the optical band gap as shown in Fig. 9. These structural changes that are being assumed, illustrate the impact generated on the electrical and optical properties, evidencing the strong correlation between the material structure and its respective properties influenced by the materials process.

## 4 Conclusion

Nanoparticles of  $\text{La}_{0.6}\text{Sr}_{0.4}\text{Co}_{0.8}\text{Fe}_{0.2}\text{O}_3$  were obtained by solution combustion synthesis using sucrose as fuel. From this study it can be concluded that sucrose as fuel is promising to synthesize LSCF by SCS when used in excess. It was demonstrated that the increase in fuel-to-oxidizer ratio modifies the crystallinity, crystallite size, morphology, and optoelectronic properties evaluated.

The excess of sucrose as fuel, after calcination at 1200 °C, allowed the synthesis of the  $\text{La}_{0.6}\text{Sr}_{0.4}\text{Co}_{0.8}\text{Fe}_{0.2}\text{O}_3$  phase with higher purity and crystallinity. On the other hand, the thermal treatment at this temperature favored an increase in crystallite size and a weight loss of more than 20% for the 1:2 sample. By the increase of fuel-to-oxidizer ratio was found a relevant variation in the conductivity of the material from  $2.61 \times 10^{-4}$  S/cm for the 1:1 to  $11.4 \times 10^{-4}$  S/cm for the 1:2 sample evaluated at 500 °C.

Furthermore, the activation energy was also lower for the 1:2 sample presenting 0.13 eV, if compared to sample 1:1 that was 0.15 eV. Lastly, the indirect band gap showed a reduction from 1.51 to 1.47 eV by the increase of fuel in SCS reaction. All these results may be attributed to the increase in the crystalline size which is driven by fuel amount in SCS of the proposed ferrite composition.

Therefore, this scientific research established an interesting relationship of synthesis parameters, such as the calcination temperature and fuel-to-oxidizer ratio which strongly influences the final characteristics of the powders obtained such as crystallinity and optoelectronic properties evaluated.

## Acknowledgements

The authors acknowledge the Brazilian National Council for Scientific and Technological Development (CNPq) and Coordination for the Improvement of Higher Education Personnel, Brasil [(CAPES)—Financial Code 001] for their financial support.

## Author contribution

All authors contributed to the study conception and design. Material preparation, data collection and analysis were performed by the authors. The new authors included in this review version contributed to improve the manuscript's suggestions and increase a detailed analysis and discussion with photophysical characterization of material and established a relationship with previous results presented in the first submitted version.

## Funding

Thais dos Santos Haas reports financial support was provided by Coordination for the Improvement of Higher Education Personnel—Brazil.

## Data availability

All data generated or analyzed during this study are included in this published article and its supplementary information files.

## Declarations

**Conflict of interests** The authors declare that they have no known competing financial interests or personal relationships that could have appeared to influence the work reported in this paper.

## References

1. Kh. Mabhouti, P. Norouzzadeh, M. Taleb-Abbasi, Effects of Fe, Co, or Ni substitution for Mn on La<sub>0.7</sub>Sr<sub>0.3</sub>MnO<sub>3</sub> perovskite: structural, morphological, and optical analyses. *J. Non-cryst. Solids* **610**, 122283 (2023). <https://doi.org/10.1016/j.jnoncrysol.2023.122283>
2. N.A. Baharuddin, H.A. Rahman, A. Muchtar, A.B. Sulong, H. Abdullah, Development of lanthanum strontium cobalt ferrite composite cathodes for intermediate- to low-temperature solid oxide fuel cells. *J. Zhejiang Univ. Sci. A* **14**, 11–24 (2013). <https://doi.org/10.1631/jzus.A1200134>
3. Y. Wu, Z. Yan, J. Xu, Z. Zhong, X. Xu, Insight into mechanism of boosted oxygen reduction reaction in mixed-conducting composite cathode of solid oxide fuel cell via a novel open-source pore-scale model. *Chem. Eng. J.* **469**, 143854 (2023). <https://doi.org/10.1016/j.ccej.2023.143854>
4. J.W. Stevenson, T.R. Armstrong, R.D. Carneim, L.R. Pederson, W.J. Weber, Electrochemical Properties of mixed conducting Perovskites La<sub>1-x</sub>M<sub>x</sub>Co<sub>1-y</sub>Fe<sub>y</sub>O<sub>3-δ</sub> (M = Sr, Ba, Ca). *J. Electrochem. Soc.* **143**, 2722–2729 (1996). <https://doi.org/10.1149/1.1837098>
5. D.P. Tarragó, B. Moreno, E. Chinarro, V.C. de Sousa, Perovskites used in fuel cells, in *Perovskite Materials, Synthesis, Characterisation, Properties, and Applications*. ed. by L. Pan (Intech Open, London, 2016), pp.619–630. <https://doi.org/10.5772/61465>
6. H. Ullmann, N. Trofimenko, F. Tietz, D. Stover, A. Ahmad-Khanlou, Correlation between thermal expansion and oxide ion transport in mixed conducting perovskite-type oxides for SOFC cathodes. *Solid State Ionics* **138**, 79–90 (2000). [https://doi.org/10.1016/S0167-2738\(00\)00770-0](https://doi.org/10.1016/S0167-2738(00)00770-0)
7. S. Lee, W. Yu, W. Jeong, T. Park, G.Y. Cho, S.W. Cha, Electrochemical study on the effect of catalytic current collecting layer on thin film La<sub>0.6</sub>Sr<sub>0.4</sub>Co<sub>0.8</sub>Fe<sub>0.2</sub>O<sub>3-δ</sub> (LSCF) cathode. *Appl. Surf. Sci.* **509**, 145224 (2020). <https://doi.org/10.1016/j.apsusc.2019.145224>
8. S.P. Jiang, Development of lanthanum strontium cobalt ferrite perovskite electrodes of solid oxide fuel cells review. *Int. J. Hydrog. Energy* **44**, 7448–7493 (2019). <https://doi.org/10.1016/j.ijhydene.2019.01.212>
9. L.W. Tai, M.M. Nasrallah, H.U. Anderson, D.M. Sparlin, S.R. Sehlin, Structure and electrical properties of La<sub>1-x</sub>Sr<sub>x</sub>Co<sub>1-y</sub>Fe<sub>y</sub>O<sub>3</sub>. Part 2. The System La<sub>1-x</sub>Sr<sub>x</sub>Co<sub>0.2</sub>Fe<sub>0.8</sub>O<sub>3</sub>. *Solid State Ionics* **76**, 273–283 (1995). [https://doi.org/10.1016/0167-2738\(94\)00245-N](https://doi.org/10.1016/0167-2738(94)00245-N)
10. P. Kaur, K. Singh, Review of perovskite-structure related cathode materials for solid oxide fuel cells. *Ceram. Int.* **46**, 5521–5535 (2020). <https://doi.org/10.1016/j.ceramint.2019.11.066>
11. M. Lubini, E. Chinarro, B. Moreno, J.R. Jurado, V.C. De Sousa, A.K. Alves, J.L.D. Ribeiro, C.P. Bergmann, Electrochemical characteristics of La<sub>0.6</sub>Sr<sub>0.4</sub>Co<sub>1-y</sub>Fe<sub>y</sub>O<sub>3</sub> (y = 0.2 – 1.0) fiber cathodes. *Ceram. Int.* **43**, 8715–8720 (2017). <https://doi.org/10.1016/j.ceramint.2017.04.002>
12. R.D. Toro, P. Hernández, Y. Díaz, J.I. Brito, Synthesis of La<sub>0.8</sub>Sr<sub>0.2</sub>FeO<sub>3</sub> perovskites nanocrystals by Pechini sol-gel method. *Mater. Lett.* **107**, 231–234 (2013). <https://doi.org/10.1016/j.matlet.2013.05.139>
13. V.C. Sousa, A.M. Segadaes, M.R. Morelli, R.H.G.A. Kiminami, Combustion synthesized ZnO powders for varistor ceramics. *Int. J. Inorg. Mater.* **1**, 235–241 (1999). [https://doi.org/10.1016/S1466-6049\(99\)00036-7](https://doi.org/10.1016/S1466-6049(99)00036-7)
14. A.P. Jamale, S. Shanmugam, C.H. Bhosale, L.D. Jadhav, Physicochemical properties of combustion synthesized La<sub>0.6</sub>Sr<sub>0.4</sub>Co<sub>0.8</sub>Fe<sub>0.2</sub>O<sub>3-δ</sub> perovskite: a role of fuel to oxidant ratio. *Mater. Sci. Semiconduct. Process.* **40**, 855–860 (2015). <https://doi.org/10.1016/j.mssp.2015.07.091>
15. L. da Conceição, A.M. Silva, N.F.P. Ribeiro, M.M.V.M. Souza, Combustion synthesis of La<sub>0.7</sub>Sr<sub>0.3</sub>Co<sub>0.5</sub>Fe<sub>0.5</sub>O<sub>3</sub> (LSCF) porous materials for application as cathode in IT-SOFC. *Mater. Res. Bull.* **46**, 308–314 (2011). <https://doi.org/10.1016/j.materresbull.2010.10.009>
16. Y.S. Chou, J.W. Stevenson, T.R. Armstrong, L.R. Pederson, Mechanical properties of La<sub>1-x</sub>Sr<sub>x</sub>Co<sub>0.2</sub>Fe<sub>0.8</sub>O<sub>3</sub> mixed-conducting perovskites made by the combustion technique. *J. Am. Ceramic Soc.* (2000). <https://doi.org/10.1111/j.1151-2916.2000.tb01410.x>
17. S.M. Khaliullin, A.A. Koshkina, Influence of fuel on phase formation, morphology, electric and dielectric properties of iron oxides obtained by SCS method. *Ceram. Int.* **47**, 11942–11950 (2021). <https://doi.org/10.1016/j.ceramint.2021.01.035>
18. M. Biswas, Synthesis of single phase rhombohedral LaNiO<sub>3</sub> at low temperature and its characterization. *J. Alloys Compd.* **480**, 942–946 (2009). <https://doi.org/10.1016/j.jallcom.2009.02.099>
19. D.P. Tarragó, C.F. Malfatti, V.C. Sousa, Influence of fuel on morphology of LSM powders obtained by solution combustion synthesis. *Powder Technol.* **269**, 481–487 (2015). <https://doi.org/10.1016/j.powtec.2014.09.037>



20. S.R. Jain, K.C. Adiga, V.R.P. Verneker, A new approach to thermochemical calculations of condensed fuel-oxidizer mixtures. *Combust. Flame* **40**, 71–79 (1981). [https://doi.org/10.1016/0010-2180\(81\)90111-5](https://doi.org/10.1016/0010-2180(81)90111-5)
21. P. Scherrer, Bestimmung der Grösse und der inneren Struktur von Kolloidteilchen mittels Röntgenstrahlen. *Nachr. Ges Wiss Göttingen* **26**, 98 (1918)
22. B. Lakshmi, B.J. Thomas, P. Gopinath, Accurate band gap determination of chemically synthesized cobalt ferrite nanoparticles using diffuse reflectance spectroscopy. *Adv. Powder Technol.* **32**, 3706–3716 (2021). <https://doi.org/10.1016/j.apt.2021.08.028>
23. S. Culas, Samuel,  $\gamma$ -Irradiation effects on the non-isothermal decomposition of strontium nitrate by model-free and model-fitting methods. *Radiat. Phys. Chem.* **86**, 90–95 (2013). <https://doi.org/10.1016/j.radphyschem.2013.01.042>
24. P. Kaur, S.K. Chawla, S.S. Meena, S.M. Yusuf, S.B. Narang, Synthesis of Co–Zr doped nanocrystalline strontium hexaferrites by sol-gel auto-combustion route using sucrose as fuel and study of their structural magnetic and electrical properties. *Ceram. Int.* **42**(13), 14475–14489 (2016). <https://doi.org/10.1016/j.ceramint.2016.06.053>
25. F.A.L. Sánchez, W.L. de Almeida, V.C. de Sousa, An investigation of fuel precursors and calcination temperature to obtain mayenite ( $\text{Ca}_{12}\text{Al}_{14}\text{O}_{33}$ ) powders by solution combustion synthesis. *Ceram. Int.* **49**, 15726–15733 (2023). <https://doi.org/10.1016/j.ceramint.2023.01.166>
26. C.M. Chanquía, L. Moggi, H.E. Troiani, Highly active  $\text{La}_{0.4}\text{Sr}_{0.6}\text{Co}_{0.8}\text{Fe}_{0.2}\text{O}_{3-\delta}$  nanocatalyst for oxygen reduction in intermediate temperature-solid oxide fuel cells. *J. Power Sources* **270**, 457–467 (2014). <https://doi.org/10.1016/j.jpowsour.2014.07.132>
27. B.J. Abdullah, Size effect of band gap in semiconductor nanocrystals and nanostructures from density functional theory within HSE06. *Mater. Sci. Semiconduct. Process.* **137**, 106214 (2022). <https://doi.org/10.1016/j.mssp.2021.106214>
28. J. Koshy, K.C. George, Annealing effects on crystallite size and band gap of CuO nanoparticles. *Int. J. Mater. Phys.* **5**, 35–42 (2014)
29. P.L.B. SILVA, R.P. Vieira, C.M. Halmenschlager, F.F. Oliveira, C.P. Bergmann, Low temperature synthesis by spray pyrolysis of  $\text{La}_{0.9}\text{Sr}_{0.1}\text{Co}_{0.2}\text{Fe}_{0.8}\text{O}_3$  thin films using ethanol and water as a solvent and their microstructural characterization. *Ceram. Int.* **41**, 13304–13309 (2015). <https://doi.org/10.1016/j.ceramint.2015.07.113>
30. I.-M. Hung, J.S. Wu, Y.W. Hsu, Y.C. Lee, Effect of morphology of  $\text{La}_{0.8}\text{Sr}_{0.2}\text{Co}_{0.2}\text{Fe}_{0.8}\text{O}_{3-\delta}$  cathode on the electrochemical performance of solid oxide fuel cell. *J. Chin. Chem. Soc.* **59**, 1329–1336 (2012). <https://doi.org/10.1002/jccs.201200164>

**Publisher's Note** Springer Nature remains neutral with regard to jurisdictional claims in published maps and institutional affiliations.

Springer Nature or its licensor (e.g. a society or other partner) holds exclusive rights to this article under a publishing agreement with the author(s) or other rightsholder(s); author self-archiving of the accepted manuscript version of this article is solely governed by the terms of such publishing agreement and applicable law.